VOLUME 1, NUMBER 8, AUGUST 2001

NANO LETTERS

Micropatterned Silica Films with Ordered Nanopores Fabricated through Photocalcination

Atsushi Hozumi,[†,‡] Hiroyuki Sugimura,[*,§] Katsumasa Hiraku,[§] Tetsuya Kameyama,[†] and Osamu Takai[*,§]

National Institute of Advanced Industrial Science & Technology, 1-1 Hirate-cho, Kita-ku, Nagoya 462-8510, Japan, and Department of Materials Processing Engineering, Graduate School of Engineering, Nagoya University, Furo-cho, Chikusa-ku, Nagoya 464-8603, Japan

Received April 26, 2001; *Revised Manuscript Received June 25, 2001*

ABSTRACT

Nanoporous silica was formed into micropatterned thin films based on the area-selective growth of silica–organic nanocomposite films and the subsequent elimination of the organic components. To eliminate organic molecules from the nanocomposite, a photochemical approach, that is, "photocalcination", using a vacuum ultraviolet light of 172 nm wavelength was employed. As confirmed by infrared spectroscopy, atomic force microscopy and X-ray diffractometry, the organic phase was completely removed from the nanocomposite by photocalcination without distorting either its well-ordered nanostructure or its finely patterned microstructures. Photocalcination is advantageous compared with the conventional thermal approach, that is, calcination, since it may be conducted at room temperature. In comparison, volume shrinkage of the silica-based nanocomposite microstructures due to photo- or thermocalcination was about 5% and 30%, respectively.

Oxides with highly ordered periodic nanopores can be prepared using surfactant assemblies as templates.[1] Such nanoporous oxides show promise to support mesostructured materials exhibiting anomalous optical, electronic, magnetic and other properties different from those of their corresponding bulk materials. For example, a variety of materials including metals, semiconductors and organic molecules have been successfully inserted into nanopores.[2] To fabricate microdevices from such nanoporous silica-based materials, they must be formed into thin films with precisely controlled geometries and morphologies. Micropatterning technologies applicable to nanoporous silica are thus of particular importance.

Ozin and co-workers have reported for the first time microfabrication of surfactant−silica nanocomposite films.[3a] Several reports related to this field have been also reported.[3b−e] After micropatterning, the organic template, that is, the surfactant assembly, must be removed from the micropatterned nanocomposite film without distorting its fine nanostructures in order to obtain ordered nanopores. In general, organic components are removed by treating a preformed

* To whom correspondence should be addressed. E-mail: sugimura@numse.nagoya-u.ac.jp. Tel.: +81-52-789-2796. Fax: +81-52-789-3259.
† National Institute of Advanced Industrial Science & Technology.
‡ E-mail: a.hozumi@aist.go.jp.
§ Nagoya University.

10.1021/nl010028o CCC: $20.00
Published on Web 07/20/2001

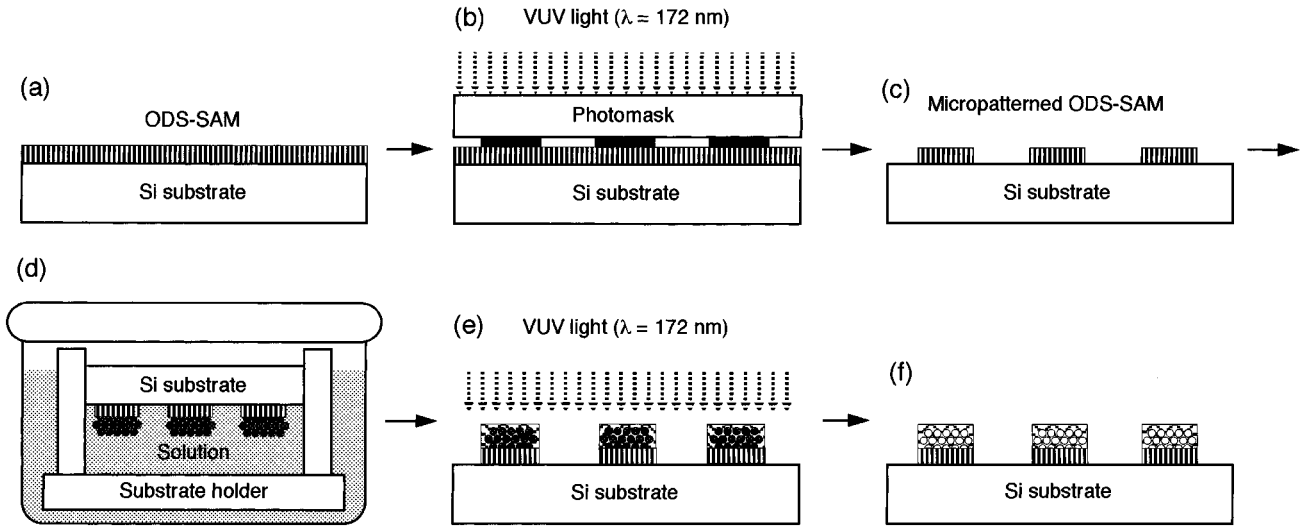

Figure 1. Schematic illustration of (a) an ODS−SAM, (b) VUV-photolithography, (c) a micropatterned ODS-SAM, (d) surfactant-silica composite film growth, (e) photocalcination, and (f) micropatterned nanoporous silica film.

nanocomposite film in air at a temperature above 300 °C. However, this conventional approach, so-called "calcination", is not suitable, particularly for thin films, since it causes marked volume shrinkage, and therefore considerable amounts of internal stress to surfactant−silica nanocomposite film. Consequently, such calcined films frequently distort and even break. An alternative method to remove organic templates from such nanocomposite films is strongly demanded. Novel approaches based on photochemistry have been reported very recently by us[4] and Clark et al.[5] Our method was based on photochemical reactions induced under irradiation with vacuum ultraviolet (VUV) light of much less than 200 nm wavelength, while Clark et al. employed oxidation with photochemically generated ozone molecules. These photochemical approaches are promising, since they can be conducted at room temperature and, thus, nanostructure distortion is much less than that caused by conventional calcination. The VUV-based method, referred to as "photocalcination", has another advantage in that silica matrices are also cured at room temperature. Photocalcination is expected to be applicable for the removal of organic templates from micropatterned nanocomposite films while preserving their microstructures, as well as for the fabrication of highly ordered nanopores.

In this letter, we investigate the applicability of photocalcination to micropatterned organic−inorganic nanocomposite films. Nanocomposite films were synthesized from cetyltrimethylammonium chloride (CTAC) and organosilicate. The films were simultaneously micropatterned on the basis of the spatially regulated growth method first reported by Ozin's group.[3a] In this study, we employed photolithographically fabricated organosilane SAM microtemplates.[6] The subsequently photocalcined samples were studied by atomic force microscopy (AFM) and X-ray diffractometry to determine, respectively, the preservation of their lithographically defined microstructures, and their ordered nanostructure regulated by the CTAC assemblies. These were compared with samples calcined by the conventional thermal method.

Micropatterned nanoporous silica films were fabricated according to the process illustrated in Figure 1. Photochemically cleaned Si substrates were first covered with an organosilane-SAM by means of a chemical vapor deposition (CVD) method using *n*-octadecyltrimethoxysilane (ODS) as a precursor (Figure 1a). The thickness of this ODS-SAM was estimated by ellipsometry to be 1.9 ± 0.1 nm. Its surface was hydrophobic, showing a water-contact angle near 110°. Details of this CVD method have been described elsewhere.[7] Next, the Si substrates coated with the ODS-SAM were photolithographically micropatterned (Figure 1b). Each ODS-SAM surface was irradiated for 30 min in a vacuum (~10 Pa) with VUV light through a photomask contacting the SAM surface. An excimer lamp (Ushio Electric UER20-172V, $\lambda = 172$ nm and 10 mW/cm^2) served as the light source. The dose rate was about 11.7 J/cm^2. Our photomask consisted of a 0.1 μm thick Cr pattern on a 2 mm thick quartz glass plate having 93% transparency at 172 nm. A 10 mm thick quartz glass plate with a transparency of about 70% at 172 nm was placed on the photomask as a weight in order to achieve satisfactory contact between the mask and the sample surface. The total light intensity at the ODS-SAM surface was estimated to be about 6.5 mW/cm^2. As confirmed by an AFM (Seiko Instruments SA300HV) in lateral force microscopy (LFM) mode using a Si probe (Park Scientific Instruments, Ultralever, force constant = 2.8 N/m), the photoirradiated regions on the ODS-SAM surface were decomposed and removed through photochemical reactions induced by the VUV irradiation, as illustrated in Figure 1c. LFM images (not shown) clearly indicated that the microstructures composed of 5 μm × 25 μm rectangular features were successfully photoprinted onto the ODS-SAM surface. A surfactant−silica composite film was synthesized onto this micropatterned ODS-SAM at room temperature in a solution prepared as follows (Figure 1d). A mixture of CTAC (Tokyo Kasei Organic Chemicals), hydrochloric acid (HCl), and water (H_2O) was stirred for about 10 min until the CTAC powder completely dissolved. Tetraethoxysilane (TEOS,

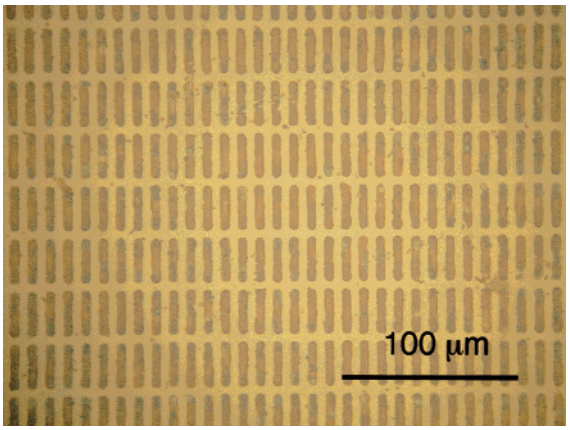

Figure 2. Optical micrograph of deposits grown on a micropatterned ODS-SAM-covered Si substrate.

Tokyo Kasei Organic Chemicals) was then added to the solution and mixed by stirring for about 2 min at room temperature. The final reactant molar ratio of TEOS/CTAC/HCl/H_2O was 0.1:0.11:7:100. The substrate was immersed upside down in this solution and kept undisturbed at room temperature for 1 h. After immersion, the substrate was washed with Milli-Q water and blown dry with N_2 gas.

An example of the deposits grown on the micropatterned ODS-SAM surface is shown in Figure 2. As clearly seen in this optical micrograph, the deposits show continuous filmlike features and have grown preferentially on the regions covered with the ODS-SAM. The unphotoirradiated regions remain almost uncovered. We confirmed by microinfrared transmission spectroscopy (IR; JASCO MICRO-20) that the micropatterned films consist of CTAC molecules and silica matrix.[4]

Since the micropattern was prepared only on a small region restricted to an area of 450 μm × 450 μm, it was difficult to measure X-ray diffraction (XRD) patterns of this region selectively. We therefore characterized the surrounding region, which was uniformly covered with the ODS-SAM and, thus, deposited with a continuous nanocomposite film. The deposits were characterized by X-ray diffractometry using Cu Kα radiation (λ = 0.154 178 nm, MAC Science MXP[3]). Its typical XRD pattern indicates one intense (100) diffraction peak with a weak (200) peak (not shown). The absence of (110) and (210) reflections in the XRD pattern shows that the channel axis of the hexagonal unit cell is oriented parallel to the ODS-SAM-covered Si surface.[1,8] The initial d_{100} values were in the range 3.2−3.7 nm.

Each of the micropatterned nanocomposite films was then directly photoirradiated under a controlled pressure of 10 Pa for 3 h by employing the same excimer lamp as used for the photolithography (Figure 1d). The dose rate was estimated to be about 70 J/cm^2. As a control experiment, identical samples were calcined thermally for 1 h in a furnace kept at a temperature of 773 K. We hereafter refer to this conventional approach as "thermocalcination". Typical micro-IR spectra obtained demonstrated that the IR absorption peaks corresponding to the C−H bonds of the CTAC molecules completely disappeared due to both the photo- and thermocalcinations. This is evidence that all the organic components were eliminated. However, the preservation of the photocalcined film's nanostructure was markedly superior compared with that of the thermocalcined film. A steady decrease in the d_{100} spacing as well as a decrease in the intensity of the (100) peak was observed in the photocalcined films. Nevertheless, the hexagonal structure remained intact, even after the organic phase was completely eliminated. This indicates that the CTAC−silica composite film was successfully converted into nanoporous silica film. On the contrary, the nanostructure of the thermocalcined film was markedly distorted. Indeed, the difference between the d_{100} values before and after thermocalcination was about 1.3 nm, a decrease of 36%. In contrast, when photocalcination was applied, the decrease in d_{100} value was significantly suppressed to be about 0.6 nm, a decrease of only 16%.

In addition to the effect of calcination on the nanostructures, its effect on the three-dimensional microstructures of the patterned composite films was studied by AFM. Parts a−c of Figure 3 show AFM images of the nanocomposite microstructures prior to calcination and after thermocalcination and photocalcination, respectively. As clearly seen in Figure 3a, the surfaces of the microstructures appear to be relatively smooth. No cracks or defects are detectable. The initial heights of the uncalcined samples were in the range 0.29−0.37 μm. The morphologies of the microstructures changed considerably due to thermocalcination. Close inspection of Figure 3b reveals that the top surfaces of the thermocalcined microstructures are no longer flat, but rather have become recessed in their central areas. The heights of these microstructures at their recessed central regions are about 0.21 μm. Since the original heights of the microstructures were about 0.37 μm before thermocalcination, the microstructures were concluded to have shrunk vertically by 27%. In contrast, Figure 3c shows the top surfaces of the photocalcined microstructures to be almost flat, similar to the uncalcined microstructures shown in Figure 3a. The observed heights of the photocalcined microstructures were estimated to be about 0.28 μm, almost unchanged from the heights of the same microstructures before photocalcination, that is, 0.29 μm. After photocalcination, the final vertical dimensions were 96% of the initial dimensions.

In addition to vertical contraction of the microstructures before and after calcinations, shrinkage in width and length were similarly estimated from the AFM images. These results are summarized in Table 1. The initial dimensions of the uncalcined microstructures were about 5.2−5.4 μm in width and 25−26 μm in length. Table 1 clearly indicates that there was little lateral contraction observable in the thermo- or photocalcined microstructures. On the basis of these results, the volumes of the thermo- and photocalcined microstructures relative to those of the uncalcined samples were calculated to be about 70% and 95%, respectively. The photocalcined microstructures shrunk much less than the thermocalcined ones.

This marked difference in volume shrinkage observed between the thermo- and photocalcined microstructures is believed to originate in the chemical reactions proceeding

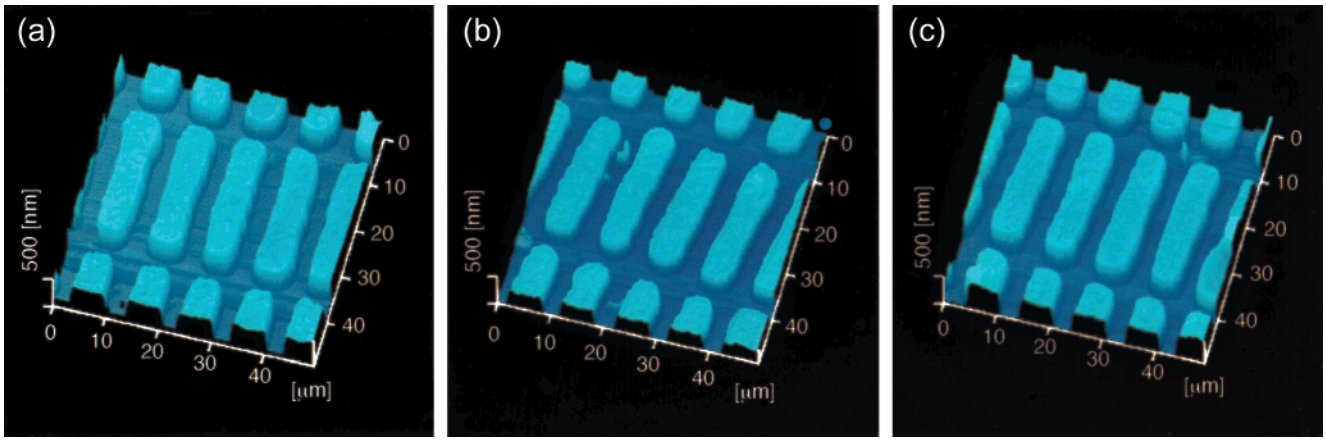

Figure 3. AFM images of the micropatterned composite films: (a) as-synthesized, (b) thermocalcined, and (c) photocalcined.

Table 1. Dimensions of the Calcined Samples Relative to the As Synthesized Sample

	width	length	height	volume
after thermocalcination (%)	100	96	73	70
after photocalcination (%)	98	100	96	95

in each of the calcinations. In the case of thermocalcination, the organic phases are eliminated from the nanocomposite microstructures due to thermal decomposition. Simultaneously, dehydration and condensation reactions proceed in the silica matrix. Indeed, we confirmed by IR that Si−OH bonds completely vanished from the thermocalcined films. Si−OH groups on silica surfaces are known to decrease at higher temperatures.[9] Our result indicates that thermocalcination allows cross-linking and consolidation of the siloxane networks to increase. On the other hand, when the microstructures are irradiated with VUV light in the presence of atmospheric oxygen, two distinct photochemical reactions proceed simultaneously at room temperature. VUV light of 172 nm in wavelength dissociatively excites chemical bonds, such as C−C, C−H, and Si−C and decomposed organic molecules.[10] Moreover, VUV light between 133 and 200 nm dissociates O_2 and generates oxygen atoms at several excited states.[11] The organic molecules that have been decomposed through the direct VUV excitation further react with these activated oxygen species and, are finally eliminated from the microstructures as volatile products, such as CO, CO_2, and NO_x.[12] As confirmed by X-ray photoelectron spectroscopy using Mg Kα radiation (AXIS HS, Shimadzu, X-ray source was operated at 10 mA and 12 kV), the carbon components were effectively removed from the samples by both calcinations. The C concentration of the samples was about 50.3 a/o before calcination, while that decreased to about 4.9 or 6.0 a/o after thermo- or photocalcination, respectively. Since the activated oxygen species have strong oxidative reactivity to the silica matrix as well as to organic molecules, the O/Si ratio of the nanocomposite films increased from 0.84 to 1.6 due to photocalcination. However, that of the thermocalcined films little changed and remained at around 1.1. It should be noted that the IR absorption intensities due to Si−OH of the photocalcined microstructures were almost identical to those of the uncalcined microstructures. Since the excimer lamp does not generate infrared rays and does not heat samples, photocalcination can be conducted at room temperature. Thus, although the silica matrix was completely oxidized and its composition approached that of pure SiO_2, siloxane networks in the photocalcined silica are thought not to be tightly packed. This may lead to the framework's flexibility of the silica matrix. This is the most probable reason: the volume shrinkage in the photocalcined microstructures was suppressed compared with thermocalcination.

In addition, it is noteworthy that vertical shrinkage dominated for both calcined microstructures, particularly, in the case of thermocalcination. These results are most likely ascribable to interactions between the composite films and the ODS-SAM surface. The silica walls in the uncalcined nanocomposite films are thought to be composed of networks of a relatively loosely cross-linked silica matrix. Because of thermocalcination, this silica matrix becomes more tightly packed, as described above, so as to contract. However, the bottom of the film is fixed to the ODS-SAM surface. Accordingly, as the silica matrix condenses due to thermocalcination, lateral contractions are greatly restricted. Thus, the micropatterned film contracts mainly in the vertical direction.

Furthermore, the percentage of height contraction of the microstructures as determined by AFM was less than the decrease in d_{100} values obtained by XRD for the unpatterned regions. Although we cannot directly compare these results, it can be firmly concluded that volume shrinkage was considerably suppressed, particularly in the case of photocalcination.

In conclusion, our results presented here offer clear evidence that photocalcination is applicable for the fabrication of micropatterned silica films with ordered nanopores. Since this process allows the elimination of organic phases from organic−inorganic nanostructured films at near room temperature, their fine microstructures can be preserved without significant distortion. This is in marked contrast to conventional calcination based on thermal decomposition of the organic phases. This novel approach we have demonstrated here will enable freer, more unrestricted design of micropatterns of nanoporous oxide materials, including

thermally unstable materials, such as transition metal oxides and phosphate analogues, and may open the path to a wide variety of advanced device applications.

References

(1) (a) Kresge, C. T.; Leonowicz, M. E.; Roth, W. J.; Vartuli, J. C.; Beck, J. S. *Nature* **1992**, *359*, 710. (b) Yang, H.; Kuperman, A.; Coombs, N.; Mamiche-Afara, S.; Ozin, G. A. *Nature* **1996**, *379*, 703. (c) Aksay, I. A.; Trau, M.; Manne, S.; Honma, I.; Yao, N.; Zhou, L.; Fenter, P.; Eisenberger, P. M.; Gruner, S. M. *Science* **1996**, *273*, 892.

(2) (a) Zhou, W.; Meurig, J.; Shephard, D. S.; Johonson, B. F. G.; Ozkaya, S.; Maschmeyer, T.; Bell, R. G.; Ge, Q. *Science* **1998**, *280*, 705. (b) Honma, I.; Zhou, H. S. *Adv. Mater.* **1998**, *10*, 1532. (c) Dag, Ö.; Ozin, G. A.; Yang, H.; Reber, C.; Bussière, G. *Adv. Mater.* **1999**, *11*, 474. (d) Marlow, F.; McGehee, M. D.; Zhao, D.; Chmelka, B. F.; Stucky, G. D. *Adv. Mater.* **1999**, *11*, 632. (e) Winkler, H.; Birkner, A.; Hagen, V.; Wolf, I.; Schmechel, R.; von Seggern, H.; Fischer, R. A. *Adv. Mater.* **1999**, *11*, 1444. (f) Wang, L.-Z.; Shi, J.-L.; Zhang, W.-H.; Ruan, M.-L.; Yu, J.; Yan, D.-S. *Chem. Mater.* **1999**, *11*, 3015. (g) Han, Y.-J.; Kim, J. M.; Stucky, G. D. *Chem. Mater.* **2000**, *12*, 2068.

(3) (a) Yang, H.; Coombs N.; Ozin, G. A. *Adv. Mater*. **1997**, *9*, 811. (b) Trau, M.; Yao, N.; Kim, E.; Xia, Y.; Whitesides, G. M.; Aksay, I. A. *Nature* **1997**, *390*, 674. (c) Yang, P.; Deng, T.; Zhao, D.; Feng, P.; Pine, D.; Chmelka, B. F.; Whitesides, G. M.; Stucky, G. D. *Science* **1999**, *282*, 2244. (d) Doshi, D. A.; Huesing, N. K.; Lu, M.; Fan, H.; Lu, Y.; Simmons-Potter, B. G., Jr.; Hurd, A. J.; Brinker, C. J. *Science* **2000**, *290*, 107. (e) Sugimura, H.; Hozumi, A.; Kameyama, T.; Takai, O. *Adv. Mater*. **2001**, *13*, 667.

(4) (a) Hozumi, A.; Yokogawa, Y.; Kameyama, T.; Hiraku, K.; Sugimura, H.; Takai, O. *Adv. Mater.* **2000**, *12*, 985. (b) Hozumi, A.; Sugimura, H.; Hiraku, K.; Kameyama, T.; Takai, O. *Chem. Mater.* **2000**, *12*, 3842.

(5) Clark, T., Jr.; Ruiz, J. D.; Fan, H.; Brinker, C. J.; Swanson, B. I.; Parikh, A. N. *Chem. Mater.* **2000**, *12*, 3879.

(6) Sugimura, H.; Ushiyama, K.; Hozumi, A.; Takai, O. *Langmuir* **2000**, *16*, 885.

(7) (a) Hozumi, A.; Ushiyama, K.; Sugimura, H.; Takai, O. *Langmuir* **1999**, *15*, 7600. (b) Sugimura, H.; Nakagiri, N. *J. Photopolym. Sci. Technol*. **1997**, *10*, 661.

(8) Sneh, O.; George, S. M. *J. Phys. Chem.* **1995**, *99*, 4639.

(9) (a) Kresge, C. T.; Leonowicz, M. E.; Roth, W. J.; Vartuli, J. C.; Beck, J. S. *Nature* **1992**, *359*, 710. (b) Sneh, O.; George, S. M. *J. Phys. Chem.* **1995**, *99*, 4639.

(10) Holländer, A.; Klemberg-Sapieha, J. E.; Wertheimer, M. R. *Macromolecule* **1994**, *27*, 2893.

(11) (a) Inoue, K.; Michimori, M.; Okuyama, M.; Hamakawa, Y. *Jpn. J. Appl. Phys.* **1987**, *26*, 805. (b) Amimoto, S. T.; Force, A. P.; Gulotty, R. G., Jr.; Wiesenfeld, J. R. *J. Chem. Phys*. **1979**, *71*, 3640.

(12) Ishikawa, Y.; Yoshima, H.; Hirose, Y. *J. Surf. Finish. Soc. Jpn*. **1996**, *47*, 74.

NL010028O